JACS
JOURNAL OF THE AMERICAN CHEMICAL SOCIETY
Article
pubs.acs.org/JACS

# CO Desorption from a Catalytic Surface: Elucidation of the Role of Steps by Velocity-Selected Residence Time Measurements

Kai Golibrzuch,[†,‡] Pranav R. Shirhatti,[†,‡] Jan Geweke,[†,‡] Jörn Werdecker,[†,‡,∥] Alexander Kandratsenka,[†,‡] Daniel J. Auerbach,[§] Alec M. Wodtke,[†,‡,§] and Christof Bartels*[,†,‡]

[†]Institute for Physical Chemistry, Georg-August University of Göttingen, 37073 Göttingen, Germany
[‡]Max Planck Institute for Biophysical Chemistry, 37077 Göttingen, Germany
[§]Department of Chemistry and Biochemistry, University of California, Santa Barbara, California, 93106, United States
[∥]Laboratoire Chimie Physique Moléculaire, École Polytechnique Fédérale de Lausanne (EPFL), CH-1015 Lausanne, Switzerland

Supporting Information

**ABSTRACT:** Directly measuring the rate of a surface chemical reaction remains a challenging problem. For example, even after more than 30 years of study, there is still no agreement on the kinetic parameters for one of the simplest surface reactions: desorption of CO from Pt(111). We present a new experimental technique for determining rates of surface reactions, the velocity-selected residence time method, and demonstrate it for thermal desorption of CO from Pt(111). We use UV−UV double resonance spectroscopy to record surface residence times at selected final velocities of the desorbing CO subsequent to dosing with a pulsed molecular beam. Velocity selection differentiates trapping-desorption from direct scattering and removes influences on the temporal profile arising from the velocity distribution of the desorbing CO. The kinetic data thus obtained are of such high quality that bi-exponential desorption kinetics of CO from Pt(111) can be clearly seen. We assign the faster of the two rate processes to desorption from (111) terraces, and the slower rate process to sequential diffusion from steps to terraces followed by desorption. The influence of steps, whose density may vary from crystal to crystal, accounts for the diversity of previously reported (single exponential) kinetics results. Using transition-state theory, we derive the binding energy of CO to Pt(111) terraces, $D_0^{\mathrm{terr}}$ (Pt−CO) = 34 ± 1 kcal/mol (1.47 ± 0.04 eV) for the low coverage limit (≤0.03 ML) where adsorbate−adsorbate interactions are negligible. This provides a useful benchmark for electronic structure theory of adsorbates on metal surfaces.

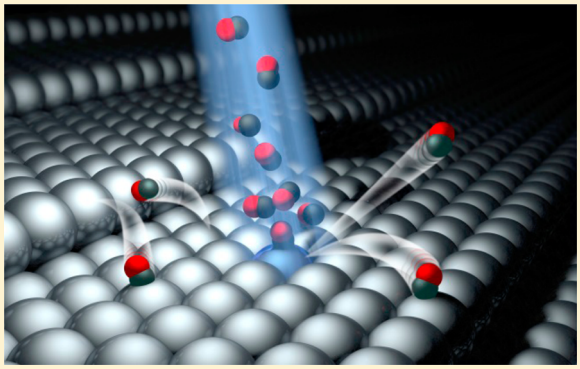

## INTRODUCTION

Desorption rates are of great practical and fundamental importance in surface chemistry and catalysis. For example, in Langmuir−Hinshelwood surface chemistry, desorption rates control surface residence times, a key kinetic influence in heterogeneous catalysis.[1] On the one hand adsorbates should stay at the surface long enough to react, and on the other hand they should desorb rapidly enough to avoid blocking adsorption sites, poisoning the catalyst.

Accurate desorption rates can also be used to derive adsorbate binding energies or desorption barrier heights. This can be seen from the desorption rate constant's surface temperature dependence, which can be derived from transition-state theory (TST):[2]

$$k_{\mathrm{d}}(T_{\mathrm{S}}) = S(T_{\mathrm{S}})\frac{k_{\mathrm{B}}T_{\mathrm{S}}}{h}\frac{Q^{\ddagger}}{Q_{\mathrm{ads}}}\mathrm{e}^{-E_0/k_{\mathrm{B}}T_{\mathrm{S}}} \quad (1)$$

Here, we need partition functions of the transition state, $Q^{\ddagger}$, and the adsorbate, $Q_{\mathrm{ads}}$. $S(T_{\mathrm{S}})$ is the sticking probability for molecules in a thermal distribution at the surface temperature, $T_{\mathrm{S}}$. It reflects the recrossing correction in TST. $E_0$ is the barrier to desorption, which in the absence of a reverse adsorption barrier is equal to the binding energy, $D_0$.

Accurate experimental binding energies are needed as benchmarks for first-principles theories of catalysis and surface chemistry.[3] A well-known example is the adsorption of CO to Pt(111). A "CO adsorption puzzle"[4] was first pointed out by Feibelman et al. and has become a major focus of theoretical work. Semilocal density functional theory (DFT) calculations for CO binding to Pt(111) are known to predict the wrong adsorption site. Furthermore, theoretical binding energies, which range from 23 to 48 kcal/mol,[5] depend strongly on the particular exchange−correlation (XC) functional.[4−6] Experiments clearly show that CO at low coverage exclusively binds on top of a Pt atom,[7] while semilocal DFT favors higher coordination and predicts higher binding energies in bridge and

Received: October 1, 2014
Published: December 1, 2014


© 2014 American Chemical Society

DOI: 10.1021/ja509530k
J. Am. Chem. Soc. 2015, 137, 1465−1475

hollow sites.[4,6a−c] The reason for this discrepancy has been traced back to strong electron delocalization errors in the semilocal XC functionals which lead to the CO's lowest unoccupied molecular orbital (LUMO) being too low in energy.[6a] Promising progress has been made with more advanced, higher-rung XC functionals, e.g., random phase approximation (RPA)-based calculations were able to predict the correct adsorption sites for CO on Pt(111) as well as Cu(111), where similar problems arose.[5,6e] However, GGA-RPA calculations are computationally expensive, limiting their application to the calculation of finite clusters. Luo et al. recently demonstrated that the meta-generalized M06-L functional[8] predicts the correct binding site and gives accurate lattice constants, surface energies, and adsorption energies.[9]

The difficulty in evaluating different theoretical approaches is compounded by the lack of consensus among experimental results on the adsorption energy of CO on Pt(111) at low coverages. In the early work of Ertl et al.,[10] the CO adsorption energy was found to be 32.3 ± 1 kcal/mol, as derived from isosteric heats of adsorption. In the direct calorimetric measurement by King et al. a significantly higher value of 45 ± 3 kcal/mol was reported.[11] In a more recent calorimetric measurement, Campbell, et al., reported a value of 31 ± 0.5 kcal/mol[12] and suggested that differences between the two calorimetric measurements might be explained by systematic errors in calibration in the earlier work due to a wrong value for the Pt(111) crystal reflectivity.

While accurate kinetics data can in principle be used to derive binding energies, in practice this has proven extremely challenging, even for the relatively simple example of CO desorption from Pt(111). Molecular beam dosing employed in combination with mass spectrometric detection of desorbing molecules has been used to obtain kinetic data for CO desorption from Pt(111).[13] Such experiments typically employ a pulsed or modulated CO molecular beam to dose the surface, while recording the time of arrival of desorbing CO at a mass spectrometer[13a] or the pressure rise phase lag.[13b,c] Other probes of CO adsorption/desorption include attenuation of specular He scattering.[13d] Similar experiments relevant to this work were performed for NO adsorption to Pt(111).[14] These methods sometimes suffer from relatively poor (ms) time resolution and/or low signal-to-noise ratio. Furthermore, the time-dependent desorption kinetics as well as the velocity distribution of the desorbing molecules may both influence the observed temporal profiles making data analysis problematic.[13a]

An additional complication may arise from atomic steps on the crystalline surface, that is, the finite size of Pt(111) terraces on any real crystal. Step sites are typically present at a density of about 0.1−3% that of terrace sites on a real crystal. Furthermore, they bind CO more strongly,[13b] and diffusion from terraces to steps is rapid compared to the time resolution of the molecular beam experiment.[14,15] Molecular beams often provide dosing conditions where the maximum CO coverage obtained is close to the density of steps (∼1% of a ML). If the dose is less than the step density, desorption may be dominated by step interactions. If the dose is above the step density, the fast terrace-to-step diffusion can lead to saturated occupation ("blocking") of step sites, and their influence on the kinetics may appear differently. These effects have been shown clearly in molecular beam kinetics on NO desorption from Pt(111).[14,15] To resolve the contribution of terraces from steps, one needs extraordinarily high signal-to-noise kinetic data under conditions where step sites are blocked[14] or where diffusion is slow compared to desorption.[14,16] The latter can be achieved at elevated surface temperatures but requires excellent temporal resolution.

In this paper, we present a new molecular beam approach to measuring desorption rates with ∼10 μs time resolution and apply it to CO desorption from Pt(111) with a measured step density of ∼0.5%. We use pulsed molecular beam dosing in combination with UV−UV double resonance spectroscopy to restrict our detection to desorbing CO molecules traveling at a defined velocity away from the surface. This allows us to selectively monitor the time-dependent flux of thermally desorbing CO molecules, removing the influence of the CO desorption velocity distribution on the time profile. The pulsed beams used in this work are quite intense; a single pulse yields a dose of $\sim 10^{14}$ molecules $cm^{-2}$, corresponding to ∼3% of a ML, allowing saturation of step sites within a single pulse of dosing while being still low enough to neglect adsorbate−adsorbate interactions. The signal-to-noise ratio is exceptionally high, revealing bi-exponential kinetic behavior: two equally important processes are seen with two distinct first-order rate constants. A kinetic model developed by Serri et al., which describes adsorption/desorption competing with diffusion between terraces and steps,[15a] is used to interpret the data. We assign the faster of the two rate processes to desorption from (111) terraces and the slower rate process to sequential diffusion from steps to terraces followed by desorption. With the help of TST, this allows us to derive binding energies for CO at Pt(111) terraces. We review the literature and recommend a value of $D_0^{terr}$(Pt−CO) = 34 ± 1 kcal/mol (1.47 ± 0.04 eV). It appears that high-level DFT calculations at the GGA-RPA level—thought to be the most accurate—underbind CO to Pt(111) by 4−6 kcal/mol, whereas DFT calculations with the meta-generalized M06-L functional are in good agreement with the experimental results.

## METHODS

**Experimental Section.** The molecular beam surface scattering machine used in this work has been described previously in detail.[17] Briefly, we generate a molecular beam by supersonic expansion of CO in a piezo-electrically driven pulsed nozzle (3 bar stagnation pressure, fwhm ∼ 150 μs, 10 Hz). The most probable speed of the beam is 790 m/s, and its mean translational energy is 0.09 eV. The beam passes two stages of differential pumping before it enters an ultrahigh vacuum chamber (base pressure $2 \times 10^{-10}$ Torr, $2 \times 10^{-9}$ Torr with the molecular beam operating). The UHV chamber is equipped with an ion detector consisting of a repeller plate, an ion lens with two cylindrical elements and a double (Chevron) microchannel plate (MCP) detector. The single-crystal Pt(111) surface is cleaned prior to every scattering experiment in a three step process: (1) 30 min of $Ar^+$ sputtering, (2) 30 min of heating to 970 K in $\sim 5 \times 10^{-7}$ Torr oxygen, and (3) annealing to 1300 K in UHV. We check for impurities using Auger electron spectroscopy. After $Ar^+$ bombardment we still detect significant amounts of carbon impurities at the surface which are removed after heating in $O_2$.

Figure 1 shows a schematic of the experimental setup for velocity selected residence time measurements. After dosing the surface with a small amount of CO from a molecular beam pulse, we detect desorbing CO molecules with a UV−UV double resonance scheme. We pump ground-state CO $X\ ^1\Sigma^+(v'' = 0)$ molecules to the metastable $a\ ^3\Pi_1(v' = 0)$ state, which has a several millisecond radiative lifetime,[18] using the output of a frequency tripled pulsed dye laser (∼3 mJ @ 206 nm, 0.1 $cm^{-1}$ bandwidth) pumped by the second harmonic of a pulsed Nd:YAG laser (pulse energy ∼250 mJ). This UV pump beam is focused with a 500 mm fused silica lens to a diameter of <1 mm and travels directly parallel to and in front of the Pt(111) surface. The


DOI: 10.1021/ja509530k
J. Am. Chem. Soc. 2015, 137, 1465−1475

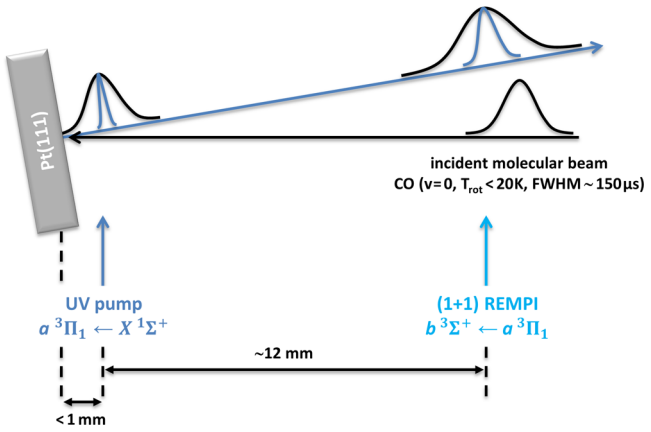


**Figure 1.** Schematic of the experimental setup for velocity resolved residence time measurements. The incident CO molecular beam is rotationally and translationally cold. It hits the surface at $\theta_i \sim 15°$. The molecules leaving the surface are tagged into the metastable $a\ ^3\Pi_1$ state <1 mm away from the surface. The metastable CO* molecules are finally detected after ~12 mm by $b\ ^3\Sigma^+ \leftarrow a\ ^3\Pi_1$ (1 + 1) REMPI. The delay between the two laser pulses is fixed and defines the velocity of the molecules being detected. The timing of the pulsed molecular beam is varied with respect to both laser pulses to observe the residence time of the molecules on the surface, detected at the selected velocity.

metastable CO* molecules are detected downstream by (1 + 1) REMPI via the $b\ ^3\Sigma^+$ ($v'' = 1$) state using a frequency-doubled pulsed dye laser (~2−3 mJ @ 265 nm, 0.1 $cm^{-1}$ bandwidth) pumped by the third harmonic of a second pulsed Nd:YAG laser. The REMPI laser beam travels antiparallel to the metastable excitation laser beam but is displaced by 12.3 mm. It is focused with a 500 mm fused silica lens to ~0.5 mm diameter.

This approach allows us to disentangle the time spread caused by residence time of the molecules at the surface from that caused by the velocity distribution of desorbing molecules by making use of two variable temporal delays, $t_1$ and $t_2$, where $t_1$ is the delay between the trigger for the CO molecular beam pulse and the UV metastable excitation laser pulse, and $t_2$ is the delay between the excitation and the detection laser pulse, defining the speed, $s_f$, of the molecules detected by REMPI. We use a fixed value of $t_2$ to select a specific velocity, $s_f \sim$ 700 m/s characteristic of desorbing CO; this enables a time-dependent CO desorption flux measurement obtained by scanning $t_1$. Alternatively, we can measure the speed distribution of the molecules by scanning $t_2$ at selected times after the pulsed CO dosing, i.e., at fixed values of $t_1$. We verified that the speed distribution of the desorbing molecules does not depend on $t_1$.

Before every measurement we flash anneal the Pt crystal to 1000 K to ensure a clean surface. In order to check for hysteresis effects related to surface contamination during the measurement, we perform $t_1$ scans "forward and backward". The absence of differences in the forward and backward scans ensures the absence of any influence of changes in surface contamination during the course of the measurements.

**Kinetic Rate Model.** For the analysis of the measured desorption time profiles, we first employed simple first-order desorption kinetics (single-exponential kinetics), allowing us to compare more easily with past work. This approach describes a mechanism of desorption from a single surface binding site. As this did not perfectly fit our data, we also implemented another kinetic mechanism, describing two first-order rate processes (bi-exponential kinetics). This mechanism describes simple desorption from terraces as well as a second rate process that involves diffusion from steps to terraces followed by desorption.

For single-exponential kinetics, we describe the CO molecular beam pulse by an empirically determined time-dependent dosing function, $\Phi_i(t)$, and the desorption of CO from Pt(111) with simple first-order kinetics, following the analysis of previous work.[13a,b,d] The number of adsorbed molecules per unit surface area, $N_{ad}(t)$, is then given by the time-dependent flux of incident and desorbing molecules:

$$\frac{dN_{ad}(t)}{dt} = \Phi_i(t) - k_d(T_S)N_{ad}(t) \quad (2)$$

The incident flux function, $\Phi_i(t)$, describes the temporal profile of the pulsed molecular beam as the sum of two Gaussian functions:

$$\Phi_i(t) = A_1 e^{-(t-t_1)^2/w_1^2} + A_2 e^{-(t-t_2)^2/w_2^2} \quad (3)$$

The two Gaussians are fitted to the measured time-dependent flux of CO molecules leaving the surface at $T_S$ = 970 K (Figure 2). At this high surface temperature, the residence time of CO on the surface (<1 μs) is much shorter than the temporal resolution of the experiment. In Figure 2, the optimized fitted dosing function (red curve) is compared to the measured temporal profile (open circles).

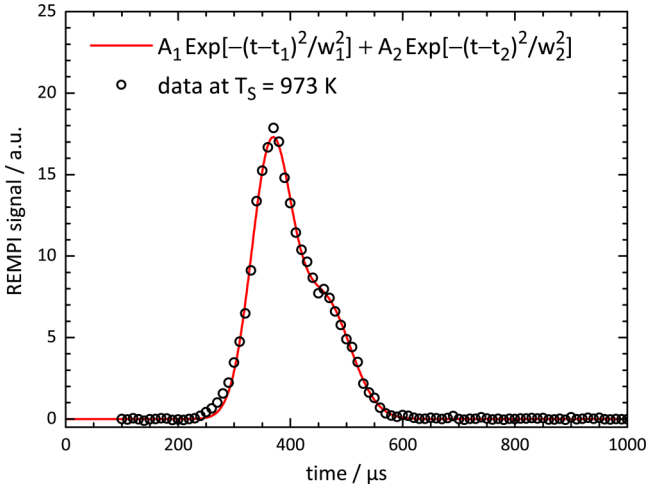


**Figure 2.** Modeling of the incident flux, $\Phi_i(t)$, of CO molecules in the kinetic model. We fit a bimodal Gaussian distribution (red curve) to the desorbing CO flux measured at a surface temperature $T_S$ = 970 K (open symbols) at which the residence time at the surface is negligible compared to the time scale of the experiment.

We plug eq 3 into eq 2 and solve for $N_{ad}(t)$ by analytical integration of eq 2 using the initial condition $N_{ad}(t = 0) = 0$. The analytic result, $N_{ad}(t)$, was found using Mathematica and is given in the Supporting Information. We then describe the flux of emerging molecules as

$$\Phi_d(t, T_S) = \underbrace{B_{DS}\,\Phi_i(t)}_{\text{direct scattering}} + \underbrace{B_{TD}\,k_d(T_S)\,N_{ad}(t)}_{\text{desorption}} \quad (4)$$

The kinetic model describes two processes: (1) a contribution resembling the dosing pulse that is independent of surface temperature and exhibits negligible residence time and (2) an exponential decay, which depends on surface temperature. The first contribution describes direct scattering of CO molecules and the second describes CO thermal desorption. We fit eq 4 to experimentally observed temporal profiles, deriving temperature-dependent rate constants, $k_d(T_S)$ as well as the branching between direct scattering, $B_{DS}$, and trapping-desorption, $B_{TD}$. In principle, the ratio $B_{DS}/B_{TD}$ between direct scattering and trapping-desorption is related to the sticking probability, $S_0$, but can deviate significantly; the experiment is quantum-state resolved, and $T_S$ dependences in the final speed or rotational distribution as well as differences in angular distribution between direct scattering and trapping-desorption can affect the $B_{DS}/B_{TD}$ ratio.

In order to describe bi-exponential kinetics, we modified eq 4 by adding a second desorption component:


DOI: 10.1021/ja509530k
J. Am. Chem. Soc. 2015, 137, 1465−1475

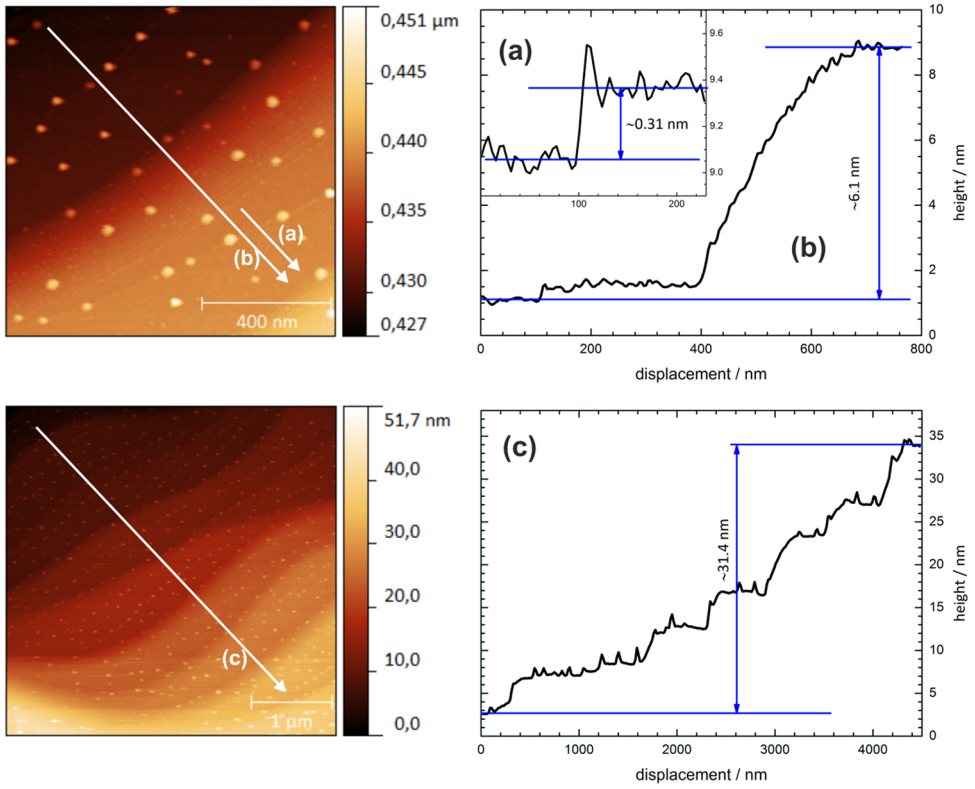


**Figure 3.** AFM images of the Pt(111) crystal used in this work for a 1 × 1 $\mu m^2$ (upper left) and 5 × 5 $\mu m^2$ (lower left) area. The plots on the right show the height profiles along the arrows (a), (b), and (c). Panel (a) shows a monatomic step with a height of about 3 Å. Panel (b) shows the effect of step bunching. Profile (c) demonstrates the height change of 31.4 nm over a distance of 4.5 $\mu m$, corresponding to an average step density of 0.5%.

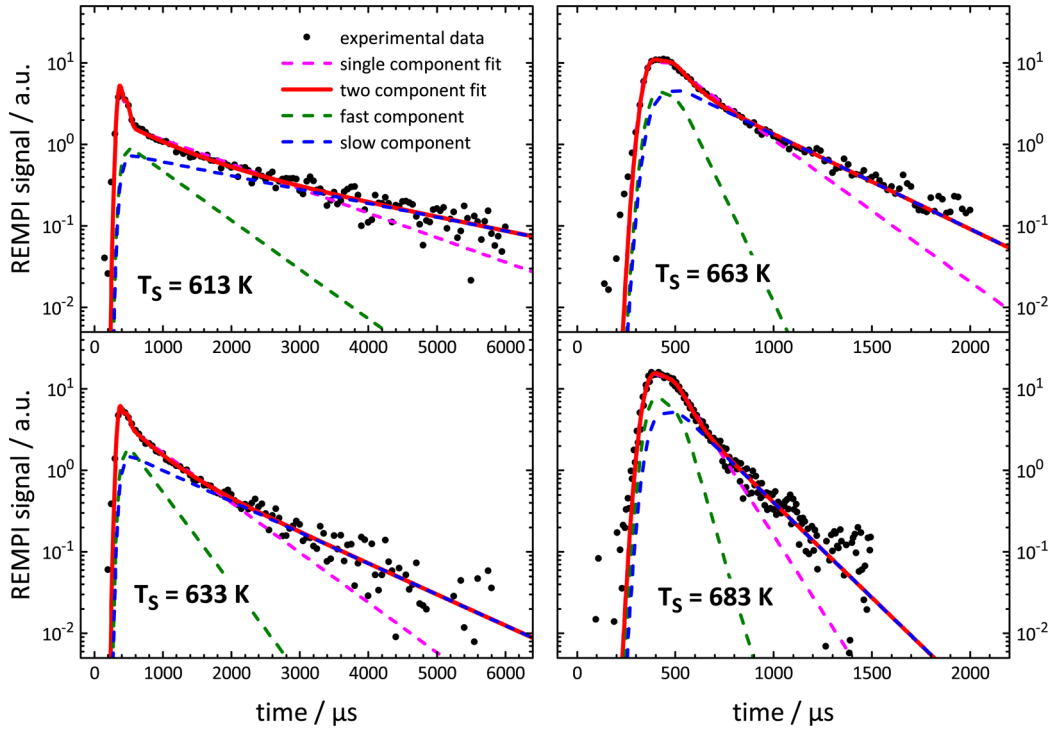


**Figure 4.** Comparison of the surface temperature-dependent velocity-selected residence time data (black dots) to two kinetic models of desorption: first-order single exponential kinetic rate model (magenta dashed curves); bi-exponential model (red curves) with fast (green dashed lines) and slow (blue dashed lines) components. The bi-exponential behavior is attributed to adsorption/desorption occurring in kinetic competition with diffusion between terraces and steps; see text.



DOI: 10.1021/ja509530k
J. Am. Chem. Soc. 2015, 137, 1465−1475

$$\Phi_d(t,T_S) = \underbrace{B_{DS}\,\Phi_i(t)}_{\text{direct scattering}} + \underbrace{B_{TD}^{fast}\,k_d^{fast}(T_S)\,N_{ad}^{(1)}(t)}_{\text{fast desorption}} + \underbrace{B_{TD}^{slow}\,k_d^{slow}(T_S)\,N_{ad}^{(2)}(t)}_{\text{slow desorption}} \quad (5)$$

**Surface Coverage and Step Density.** Important parameters in the experiment are the surface coverage caused by the pulsed CO molecular beam dosing, and the step density of the Pt surface. Based on the steady-state pressure in the UHV chamber and the pumping speed, we estimate a CO dose of ~$1 \times 10^{14}$ molecules pulse$^{-1}$ cm$^{-2}$ corresponding to ~0.03 ML per pulse, assuming that each Pt atom corresponds to one binding site. Consequently, our experiments represent the low coverage regime where adsorbate−adsorbate interactions are negligible.

We estimate the step density of the Pt(111) surface using atomic force microscopy (AFM). The left panels of Figure 3 show AFM images of $1 \times 1$ $\mu$m$^2$ (top) and $5 \times 5$ $\mu$m$^2$ (bottom) areas. We observe a high density of particles at the surface, probably resulting from exposure of the sample to air, which we ignore in the step density analysis. The panels on the right show height profiles along the arrows (a), (b), and (c). The profile (a) illustrates the presence of monatomic steps with a height of ~3 Å, in good agreement with the Pt−Pt distance of 2.7 Å.[19] Panel (b) demonstrates the effect of step bunching,[20] that is the accumulation of a high density of steps at the surface. We observe a flat terrace (displacement 150−400 nm) followed by a high density of steps (400−700 nm). For estimation of the average step density, we use profile (c). The height of the surface increases by about 31 nm over a distance of 4.5 $\mu$m, corresponding to ~100 monatomic steps within $2 \times 10^4$ rows of Pt atoms (2.4 Å distance between two rows of atoms). Consequently, we obtain a step density of 0.5% for a $5 \times 5$ $\mu$m$^2$ area.

Note that the surface has areas with a higher density of steps and that one cannot examine the entire surface with AFM. Therefore, we estimate the density of steps to be in the order of 0.5−1%, which is still lower than the dosing of the molecular beam. Consequently, the molecular beam is able to saturate the step sites. It is of course conceivable that with respect to diffusion, step bunches may behave quite differently than single steps; however such differences will be neglected in all subsequent analysis modeling the surface as uniform terraces separated by monatomic steps.

## RESULTS

Figure 4 shows experimentally measured CO flux distributions, where $t_2$ is chosen to select a speed $s_f$ = 721 m/s; data are shown for $T_S$ = 613−683 K. The useful range of surface temperatures is limited by two factors: (1) at low $T_S$, by the signal-to-noise ratio, as desorption is slow, and (2) at high $T_S$, by the temporal width of the pulsed molecular beam, which defines the time resolution of the experiment. We are also careful to operate only at high enough $T_S$ that CO fully desorbs between molecular beam pulses.

Figure 4 shows fits of the single-exponential model, eq 4 (magenta dashed lines), and the bi-exponential model, eq 5 (red solid lines), to the experimental data. The two contributions to the bi-exponential fit are indicated as green dashed and blue dashed curves. At all surface temperatures, we find that the data deviates from a single-exponential decay. The single-exponential fit reproduces the observed data at early times but fails to describe the second slower kinetic process appearing at later times.

Despite these deviations at later times, we may nevertheless attempt to fit the data to a single-exponential model. Although clearly incorrect, it will allow us to compare to previous experiments where the data were modeled with single exponential decay. The resulting rate constants, $k_d$, are shown as black circles in Figure 5 as an Arrhenius plot. The error bars reflect 90% confidence intervals. We extract activation energy,

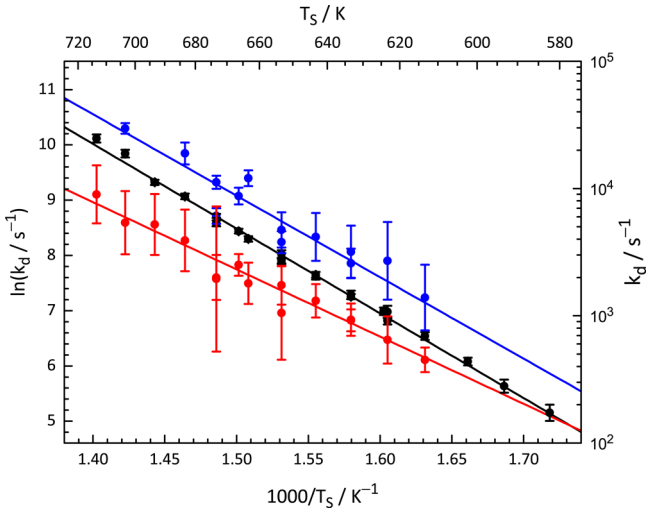


**Figure 5.** Rate constants obtained in this work as Arrhenius plots. Red and blue circles result from the bi-exponential fitting to the data. We assign the faster of the two rate processes ($k_d^{fast}$, blue circles) to desorption from Pt(111) terraces, and the slower rate process ($k_d^{slow}$, red circles) to sequential diffusion from steps to terraces followed by desorption. Black circles result from a single-exponential fit, reflecting simple first-order kinetics. While these rate constants do not fit the data as well as the bi-exponential, they can be used for comparison to previous work, which all used single-exponential fitting. The error bars reflect 90% confidence intervals.

$E_d$, and pre-exponential factor, $\nu$, from the slope and the intercept of a linear fit to the data, weighted by the uncertainty in ln $k_d$. We obtain the following values: $E_d$ = 1.32 ± 0.04 eV and $\nu = (4.7^{+4.9}_{-2.4}) \times 10^{13}$ s$^{-1}$, where the errors reflect 90% confidence intervals. From the fit, we also obtain the branching ratio between direct scattering and trapping-desorption $B_{DS}/B_{TD}$ = 0.24 ± 0.01, which is approximately independent of $T_S$.

The single-exponential first-order model clearly fails to reproduce data like that shown in Figure 4, whereas a bi-exponential model does much better. The bi-exponential fit yields two temperature-dependent rate constants, $k_d^{fast}(T_S)$ and $k_d^{slow}(T_S)$. In fitting to the bi-exponential model, eq 5, we reduced the number of variable fit parameters. Specifically, we used a constant direct scattering contribution (constant $B_{DS}$); this is consistent with the observation that $B_{DS}/B_{TD}$ was found to be independent of $T_S$ in the single exponential fitting. We note that the time integrated contributions to the signal of the fast and slow desorption components are nearly equal, $B_{TD}^{fast}/B_{TD}^{slow} \sim 1$, for the whole range of surface temperatures studied.

Figure 5 shows the Arrhenius analysis of the two rate constants, $k_d^{fast}(T_S)$ and $k_d^{slow}(T_S)$, yielding $E_d^{fast}$ = 1.27 ± 0.07 eV and $\nu^{fast} = (3.5^{+7.2}_{-2.7}) \times 10^{13}$ s$^{-1}$ for the fast component (blue), and $E_d^{slow}$ = 1.05 ± 0.10 eV and $\nu^{slow} = (1.9^{+28}_{-0.1}) \times 10^{11}$ s$^{-1}$ for the slow component (red).

In summary, we observe clear evidence of bi-exponential behavior in the desorption of CO from a Pt(111) crystal with 0.5−1% step density. The early part of the data can be fitted to a single-exponential kinetic model in order to compare to previous work. The bi-exponential fitting yields better agreement with the experimental data, providing a set of fast and slow rate constants that are higher and lower than the single exponential rate constants, respectively.


DOI: 10.1021/ja509530k
J. Am. Chem. Soc. 2015, 137, 1465−1475

## ■ ANALYSIS AND DISCUSSION

Investigating the interactions of CO with Pt(111) has attracted much attention both from experimentalists[7c,10,13,21] and theoreticians.[4−6] Experimental studies have focused on non-dissociative adsorption of CO on the Pt surface investigating desorption rates and adsorption sites.[7c,10,13a,b,d,21b−f,22] Using a variety of methods to obtain Arrhenius parameters, remarkably different results have been reported (see Table 1). The reported activation energies for desorption, $E_d$, range from 1.0 to 1.5 eV, while less effort has been made to evaluate the pre-exponential factor, $\nu$, reports of which range over 2 orders of magnitude.[13a,b,d]

**Table 1. Overview of Results from This and Previous Studies Aimed at Measuring Desorption Kinetics of CO from Pt(111)[a]**

| activation energy $E_d$, eV | pre-exponential factor $\nu$, $s^{-1}$ | method | reference |
|---|---|---|---|
| 1.32 ± 0.04 | $(4.7^{+4.9}_{-2.4}) \times 10^{13}$ | velocity resolved residence time measurements (first-order kinetic assumption) | this work |
| 1.27 ± 0.07 | $(3.5^{+7.2}_{-2.7}) \times 10^{13}$ | velocity resolved residence time measurements (terrace desorption) | this work |
| 1.05 ± 0.10 | $(1.9^{+2.8}_{-0.1}) \times 10^{11}$ | velocity resolved residence time measurements (slow component) | this work |
| 1.297 | $2.9 \times 10^{13}$ | modulated MB scattering | 13b |
| 1.349 | $2.7 \times 10^{13}$ | specular He scattering | 13d |
| 1.39 | $4.3 \times 10^{14}$ | modulated MB scattering | 13a |
| 1.51 | $1.25 \times 10^{15}$ | modulated MB scattering[b] | 13c |
| 1.38 | $1.4 \times 10^{14}$ | thermal He scattering | 29 |
| 1.21 | $(10^{13})$ | TPD | 10 |
| 1.17 | $(10^{13})$ | TPD | 30 |
| 1.28 | $(10^{13})$ | TPD | 31 |
| 1.50 | – | TPD | 7c |

[a]Shown are activation energies for desorption and pre-exponential factors of the Arrhenius equation. When pre-exponential factors were assumed, they are in parentheses. [b]The authors used a Pt(111) crystal with ∼5% step density, significantly higher than the dose of the modulated molecular beam.

**Comparison to Previous Work.** There are four molecular beam-based experiments reported in the literature, to which our results might best be compared. Winicur et al.[13d] used attenuation of specular He scattering as a probe of CO coverage; in this way the temporal decay of steady-state CO coverage could be seen when the CO beam was modulated. This method had millisecond time resolution, restricting the temperature range to $T_S \leq 600$ K. Lin and Somorjai[13b] as well as Campbell et al.[13c] used modulated molecular beam scattering and observed the phase lag of the CO pressure rise in the interaction chamber. Verheij et al.[13a] used a similar modulated beam technique but applied a pulse shape analysis to the time-dependent CO pressure profiles. While similar in principle and design, even these four studies gave quite different results: reported $E_d$ values vary by ∼0.2 eV and pre-exponential factors vary by 2 orders of magnitude; see Table 1.

We used the activation energies and pre-exponential factors reported in these four studies to compare to our derived rate constants in the temperature range of this work; see Figure 6. It is interesting to note that the rate constants from previous work, all derived from single exponential decay analysis, fall within the range set by the fast and slow processes making up the bi-exponential kinetics seen in this work. This suggests that some uncontrolled conditions in the previous experiments make them more or less sensitive to one or the other of the two rate processes identified and resolved in this work.

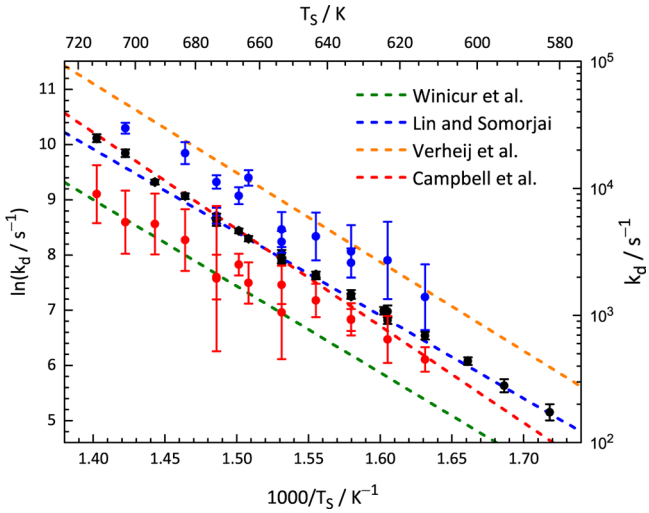


**Figure 6.** Comparison of previously reported rate constants to the present work. The black, red, and blue circles are the same as in Figure 5. Our results are compared to four previous molecular beam-based kinetics studies; see text.

The results from both Campbell et al. and from Lin et al. suggest that they may have had quite similar conditions as in this study; the single exponential analysis of their data is nearly identical to the single exponential analysis of our data. However, Campbell et al. determined the step density of their Pt(111) crystal to be about 5%, significantly lower than the dose of the molecular beam, which makes this interpretation questionable. Verheij et al. appear to have created conditions that are mostly sensitive to the faster of the two processes resulting from a very low step density (∼0.1%) of the Pt(111) crystal in that study; Winicur et al. appear to be more sensitive to the slower of the two processes.

We will show results below that suggest that this uncontrolled experimental condition is the ratio of CO dose to step density. When CO doses are high compared to step density such that the more strongly binding steps are saturated with CO, kinetics from terraces is seen. When CO doses are small compared to step density, fast diffusion from terraces to steps occurs, and the desorption kinetics are dominated by a sequential process involving first diffusion from step to terrace followed by desorption. Simple desorption from steps can be neglected due to the low concentration of step sites at the surface: The high sticking probability of CO to Pt(111) indicates that adsorption predominantly occurs at terraces. According to the principle of detailed balance, desorption will then also occur predominantly from terrace sites.[15a]

**Deviation from First-Order Kinetics: The Role of Steps and Surface Coverage.** We now explain the origin of the bi-exponential kinetics seen in this work, which involves surface diffusion between steps and terraces in kinetic competition with adsorption and desorption from terraces. Exactly this phenomenon has been previously studied experimentally for NO desorption from Pt(111),[14] and a kinetic model was developed.[15a] Together, theory and experiment clearly demonstrated the role of step sites in experiments designed to measure the rate of desorption from terraces of single


DOI: 10.1021/ja509530k
J. Am. Chem. Soc. 2015, 137, 1465−1475

crystals with a few percent step densities. The importance of steps arises first because molecules tend to bind more strongly there[13b] and second because molecular beam dosing typically produces transient surface concentrations smaller than or similar to the step density. Under conditions where the dose is less than the step density, adsorption at terraces is followed by rapid diffusion to steps and the observed desorption is a sequential (single exponential) process involving first diffusion back to the terrace and then desorption. Under conditions where dosing results in the step sites being saturated, (single exponential) desorption from terraces can be seen. Hence depending on the occupation of step sites, quite different rates can be observed.[14]

We apply the kinetic model of ref 15a to the CO/Pt(111) system. The time-dependent rates into and out of a specific adsorption site are given by the eqs 6−8:

$$\dot{\eta}_0(t) = -2k_S\eta_0(t) + 2k_H(1 - \gamma\eta_0(t))\eta_1(t) \quad (6)$$

$$\dot{\eta}_1(t) = k_S\eta_0(t) - [k_T + k_H(2 - \gamma\eta_0(t))]\eta_1(t) + k_H\eta_2(t)$$
$$\vdots \quad (7)$$

$$\dot{\eta}_m(t) = -(k_T + 2k_H)\eta_m(t) + k_H(\eta_{m-1}(t) + \eta_{m+1}(t)) \quad (8)$$

where $\eta_0$ corresponds to the population at a step site, $\eta_1$, ..., $\eta_m$ reflect the population at the 1st, ..., $m^{th}$ terrace adsorption site, and $\gamma$ is an occupancy factor that denotes step saturation. The model contains three different rate constants: $k_H$ is the rate constant for site-to-site hopping on the (111) terraces, $k_S$ is the rate constant for step-to-terrace hopping, and $k_T$ is the rate constant for desorption from the terrace sites.

The site-to-site hopping rate constant on the terraces, $k_H$, has been measured previously. Reutt-Robey et al.[15b] observed temperature-dependent hopping rates in the range $T_S$ = 95−195 K. The observed Arrhenius expression, $k_H(T_S) = (8 \times 10^9\ s^{-1})e^{-0.19eV/k_BT_S}$, yields hopping rates on the order of $2 \times 10^9\ s^{-1}$ in the temperature range of this work, 580−720 K. An earlier study of Poelsema et al. using specular He scattering estimated parameters yielding about 10 times higher hopping rates[23] − our results show that higher $k_H$ does not affect the model since diffusion is much faster than desorption. Next, we postulate that the rate constant for terrace desorption, $k_T$, corresponds to the fast component in Figure 4; it follows the expression $k_T(T_S) = (3.5 \times 10^{13}\ s^{-1})e^{-1.27eV/k_BT_S}$. The step-to-terrace hopping rate constant, $k_S$, is unknown. For NO/Pt(111), Serri et al. assumed that the activation energy for this process is equal to the activation energy for $k_H$ plus the difference in binding energies for CO at step and terrace sites. We estimate the latter from the comparison of CO desorption from Pt(111) and Pt(557) by Lin and Somorjai;[13b] the authors obtained a 0.16 eV higher activation energy for the stepped high-index surface. Furthermore, we use the assumption of Serri et al. that the prefactor for step-to-terrace hopping is about an order of magnitude lower than for $k_H$. Consequently, we obtain a temperature-dependent rate constant $k_S(T_S) = (5 \times 10^8\ s^{-1})e^{-0.35eV/k_BT_S}$. The nonlinear system of coupled differential equations (eqs 6−8) can be solved numerically without further assumptions. Figure 7 shows the results for 0.5% step density and initial surface coverage below (upper panel) and above (lower panel) the step density. At early times, we always find a fast decay (with <5 $\mu$s time constant) of the desorbing flux, resulting from molecules initially adsorbed at the terraces

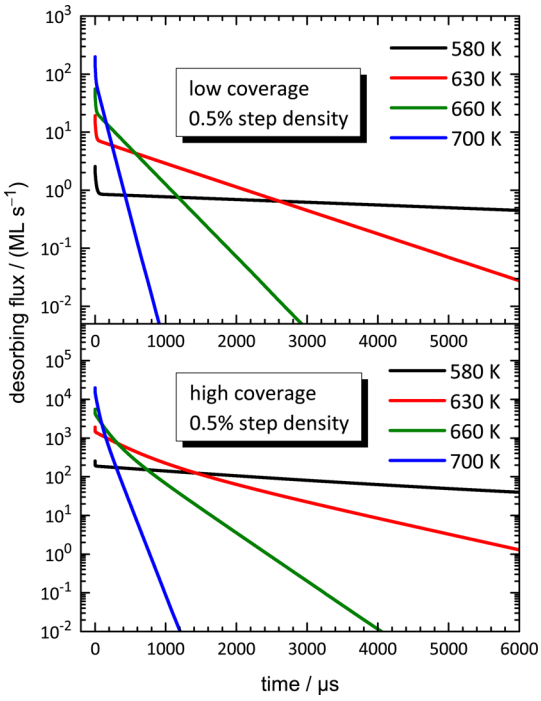


**Figure 7.** Simulation of the desorption kinetics for CO from Pt(111) based on the model of Serri et al.[15a] for 0.5% step density at four different surface temperatures, $T_S$ = 580, 630, 660, and 700 K. The upper panel shows the results for an initial surface coverage lower than the step density, while the lower panel shows results for a surface coverage that exceeds the density of step sites.

rapidly diffusing to the steps. At low coverage, this fast decay is followed by a single-exponential decay corresponding to step-to-terrace diffusion and subsequent desorption from the terraces. In the high coverage regime, where step sites are initially saturated, we find a bi-exponential decay of the desorbing flux similar to our experimental observations.

The rate constants for the two processes making up the bi-exponential decay of the model are shown as dashed lines in Figure 8. The fast component (blue dashed line) agrees very well with the experimental values of $k_d^{fast}$ (blue symbols), which were used to calculate $k_T$. Therefore, we attribute this feature to direct desorption of CO molecules from the terrace sites after step saturation. The slow component (red dashed line) is in reasonably good agreement with the experimental $k_d^{slow}$ values (red symbols) and is identical with the desorption rate at low coverage. It reflects the process of step-to-terrace diffusion followed by desorption from the terrace sites. Note that the rate constant for this process depends on the assumed step density, whereas the rate constant for direct terrace desorption does not. Increasing the step density to 1% decreases the slow rate constant almost by a factor of 3; this is also shown in Figure 8 as a red dotted line. The effective rate constant, $k_{eff}$, for a given incident flux, $SI$, of adsorbing molecules has been evaluated by Serri et al.:[15a]

$$k_{eff} = \frac{k_T}{1 + \left(\frac{\mu}{1-\mu}\right)\frac{k_H}{k_S}\left(1 + \gamma\frac{k_H}{k_Sk_T}SI\right)^{-1}} \quad (9)$$

with the rate constants for terrace desorption, $k_T$, site-to-site hopping on the terraces, $k_H$, and step-to-terrace hopping, $k_S$, the step density, $\mu$, the occupancy factor, $\gamma$, and incident adsorbing flux at each adsorption site, $SI$. For high incident fluxes (high


DOI: 10.1021/ja509530k
J. Am. Chem. Soc. 2015, 137, 1465−1475

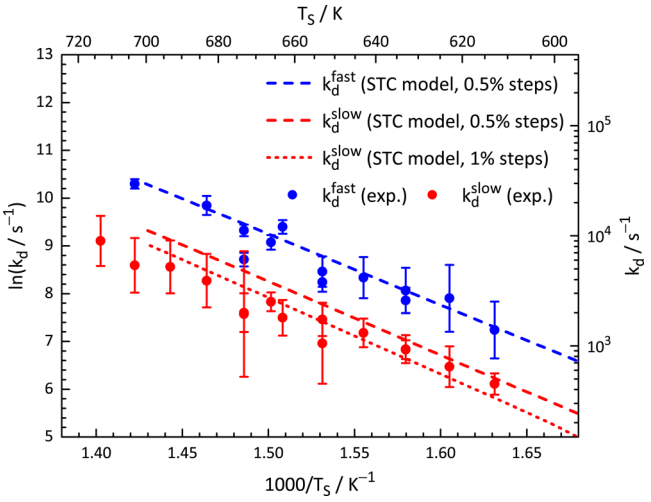


**Figure 8.** Comparison of experimental rate constants, $k_d^{fast}$ (blue symbols) and $k_d^{slow}$ (red symbols), to the slow (red) and fast (blue) component of the bi-exponential decay in the simulations of Figure 7. The fast component agrees well with the experimental value of $k_d^{fast}$. The slow component is in good agreement with the experimental rate constants for $k_d^{slow}$. The slow rate constant depends on the assumed step density in the model while the fast rate constant is independent of the density of steps.

coverage, $\gamma k_H k_S^{-1} k_T^{-1} SI \gg 1$), $k_{eff}$ becomes equal to the terrace desorption rate (fast component). At low coverage ($\gamma k_H k_S^{-1} k_T^{-1} SI \ll 1$), eq 9 can be approximated by

$$k_{eff,low} = \frac{k_T}{1 + \left(\frac{\mu}{1-\mu}\right)\frac{k_H}{k_S}} \tag{10}$$

Evaluation of the effective activation energy ($E_{d,eff} = -k_B d \ln k_{eff}/dT^{-1}$) yields an expression that depends on the density of steps as well as on the activation energies and pre-exponential factors for $k_T$, $k_H$, and $k_S$. Evaluation of the effective pre-exponential factor yields a similarly complex expression. The complexity of the expression may lead to the unusually low pre-exponential factor and activation energy for the slow desorption component observed in the experiment. Based on the comparison of the experimental rate constants to the adsorption/desorption model of Serri et al., we conclude that the fast desorption process observed in the experiment can be assigned to direct desorption from terrace sites. We note that a bi-exponential decay of the desorbing flux is only observable if the surface dose of the molecular beam is high enough to saturate the steps at the surface. Otherwise, the system will show first-order desorption kinetics, reflecting step-to-terrace diffusion followed by terrace desorption.

This conclusion is different than the interpretation of bi-exponential desorption kinetics recently reported in the work of Starr et al.[16] for Pb desorption from Mo(100). In that work, the faster of the two rate processes—assigned to direct desorption from steps—exhibited a high activation energy but an unusually large pre-exponential factor ($9.4 \times 10^{19}$ $s^{-1}$). The slower process—assigned to direct desorption from terraces—exhibited a lower prefactor ($5.1 \times 10^{15}$ $s^{-1}$) and activation energy, the latter of which was compared with a micro-calorimetry-derived binding energy for Pb on Mo(100) terraces.[24] The large ratio of pre-exponential factors (>$10^4$) was explained as an entropy-driven desorption involving adsorbates at steps and terraces that behave as 1D and 2D gases, respectively.[16] A major difference to the present work was the assumption that diffusion between steps and terraces was unimportant; it was estimated to be slower than the 0.1 s measurement time in the Pb/Mo(100) experiment. For CO/Pt(111), CO diffusion between steps and terraces is known to be rapid (nanosecond time-scale under our conditions),[15] hence an atomic scale model of diffusion mediated desorption must be applied. We also note that the ratio of the pre-exponential factors for the fast and slow processes in this work ($10^2$) is much smaller than expected for an entropy-driven desorption; the ratio is expected to be ~5000 based on eq 1 in ref 16 for CO/Pt(111) at 650 K with 0.8% step density. Finally our assignment of the faster process to terrace desorption is consistent with a previous CO desorption study where sulfur was used to block steps on a Pt(111) surface.[25]

The analysis of the effective rate constant for desorption (eqs 9 and 10) already showed that the simple statement "a higher activation energy indicates stronger binding" is not true for CO adsorbed on Pt(111). The lower activation energy for the slow desorption component may result from the fact that it does not reflect a single-step process anymore, which leads to unexpectedly low Arrhenius parameters. In case of Pb/Mo(100), the situation might be different due to the very low mobility of the Pb atoms, different coordination number or the different surface structure.

Returning to our discussion of the previous work (Figure 6) it now appears likely that the various experiments were carried out under conditions of different levels of step-site saturation. It would appear that the Winicur et al. conditions involved unsaturated step sites, for Verheij et al. step sites appear saturated, and for Lin et al. as well as Campbell et al. it appears their conditions may have been similar to the conditions of our experiments. Of course, there may be other factors that lead to the disagreement between these various studies.

**Derivation of the Binding Energy.** For comparison to first-principles theory it is necessary to calculate the binding energy, $D_0$, of the molecule to the surface. We apply TST to fit our experimental rate constants for terrace desorption, $k_d^{fast}$. The standard TST expression, as given in eq 1, has been worked out by Tully.[2] In absence of an activation barrier, as suggested by the incidence energy-dependent sticking probability measurements,[21b] the transition state corresponds to the gas-phase molecule (eq 11) and the TST barrier height, $E_0$, is equal to the binding energy, $D_0$. The partition function for the adsorbate, $Q_{ad}$, and the transition state, $Q^{\ddagger}$, can be calculated from statistical mechanics.

$$Q^{\ddagger}(T_S) = \underbrace{\frac{2\pi m k_B T_S}{h^2}}_{Q_{trans}^{2D}} \times \underbrace{\frac{8\pi^2 I_{CO} k_B T_S}{h^2}}_{Q_{rot}} \times \underbrace{\frac{1}{1 - e^{-\frac{h\nu_{CO}}{k_B T_S}}}}_{Q_{vib}} \tag{11}$$

Note that eq 11 contains a 2D partition function for the translational motion; the motion normal to the surface corresponds to the reaction coordinate and is separated in the frequency factor, $k_B T_S/h$. The partition function of the adsorbate can be written in two ways: (1) all vibrational modes can be treated as harmonic oscillators or (2) the motion parallel to the surface can be treated as free 2D translation, eqs 12 and 13:

$$Q_{ad}^{osc}(T_S) = N_{sites} \times \prod_{i=1}^{4} \left(\frac{1}{1 - e^{-h\nu_i/k_B T_S}}\right)^{g_i} \tag{12}$$



DOI: 10.1021/ja509530k
J. Am. Chem. Soc. 2015, 137, 1465−1475

$$Q_{ad}^{2D} = Q_{trans}^{2D} \times \frac{1}{1 - e^{-h\nu_1/k_B T_S}} \times \frac{1}{1 - e^{-h\nu_2/k_B T_S}} \quad (13)$$

with the vibrational frequencies: $\nu_1$ = 2100 cm$^{-1}$ (CO stretch), $\nu_2$ = 480 cm$^{-1}$ (Pt-CO stretch), $\nu_3$ = 411 cm$^{-1}$ (hindered rotation), and $\nu_4$ = 48.5 cm$^{-1}$ (hindered translation),[21c,26] and the degeneracies $g_1$ = 1, $g_2$ = 2, $g_3$ = 2, and $g_4$ = 2, respectively. The two assumptions yield the following TST expressions:

$$k_{TST}^{osc}(T_S) = S(T_S) \times \frac{k_B T_S}{h} \times \frac{Q^{\ddagger}(T_S)}{Q_{ad}^{osc}(T_S)} \times e^{-E_0/k_B T_S} \quad (14)$$

$$k_{TST}^{2D}(T_S) = S(T_S) \times \frac{k_B T_S}{h} \times \frac{Q^{\ddagger}(T_S)}{Q_{ad}^{2D}(T_S)} \times e^{-E_0/k_B T_S} \quad (15)$$

We assume the sticking probability $S(T_S)$ to be independent of surface temperature as suggested by similar sticking probabilities of $S$ = 0.7−0.85 derived at $T_S$ = 350 K[21b] and at higher surface temperatures.[13b,c] We estimated the temperature dependence from the $E_I$ dependent sticking probabilities of Harris and Luntz[21b] but found no significant influence on $E_0$. The dependence on the absolute value of $S$, although its effect on $E_0$ is weak, is still larger than the estimated effect of surface temperature. We use a sticking probability of $S$ = 0.73 as obtained in a recent study.[12] Figure 9 shows the fits of eq 14

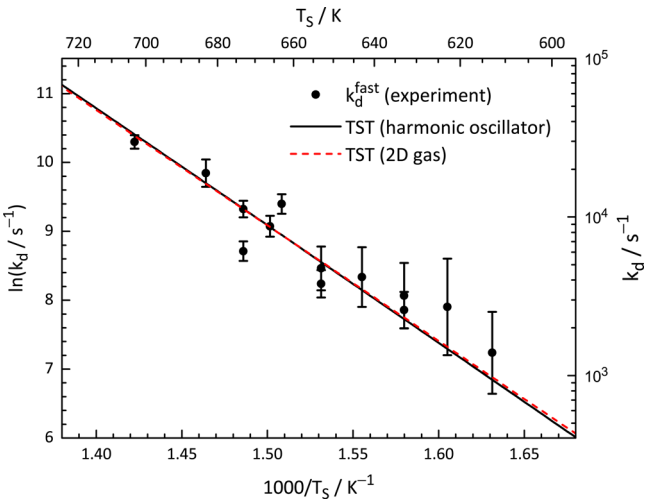


**Figure 9.** Comparison of TST to observed rate constants for CO desorption from Pt(111) terraces. Experimentally derived rate constants are shown as black circles. Two assumptions for the adsorbate partition function are shown: harmonic oscillator as in eq 12 (black solid line) and 2D translation as in eq 13 (red dashed line). These two assumptions result in slightly different CO-Pt(111) binding energies; see Figure 10.

(black solid line) and eq 15 (red dashed line) to the experimental fast rate constants, $k_d^{fast}$, which was assigned to desorption from terraces. We derive binding energies of $D_0^{osc}$ = 1.51 ± 0.01 eV (34.8 ± 0.2 kcal/mol) and $D_0^{2D}$ = 1.43 ± 0.01 eV (33.0 ± 0.2 kcal/mol), respectively. The errors indicate the statistical uncertainty of the fit.

While the statistical error is extraordinarily small, the systematic error introduced by the use of TST is much larger. In a general sense, there remains uncertainty in the application of TST to CO desorption from Pt(111). TST has not been extensively tested for surface chemical reactions; however, comparison of TST to experiment for gas-phase reactions has been very successful.[27] We see no fundamental reason why TST would work better for gas-phase reactions in comparison to surface reactions. Nevertheless, future work to test the validity of TST in surface reactions would be highly desirable. More specifically, it is not obvious which choice of adsorbate partition function mentioned above is superior. This is an important question as this is the largest source of systematic error in deriving the CO binding energy. We have shown two limiting calculations; the true partition function would yield a result between them. Hence, the average of these two values is our recommended result, and their difference introduces systematic uncertainty: $D_0$ = 1.47 ± 0.04 eV (34 ± 1 kcal/mol). Should the ambiguity in the choice of partition function be removed, the error bar might be significantly smaller.

Figure 10 shows a comparison of the experimentally derived binding energies of this work to heats of adsorption obtained by

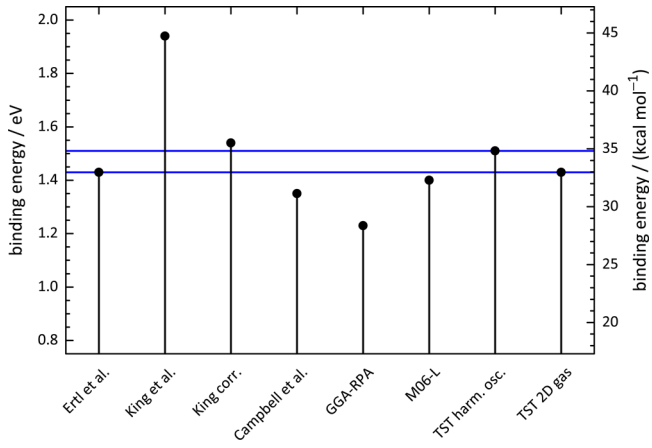


**Figure 10.** Binding energy of CO to Pt(111). The blue lines indicate our recommendation, 34 ± 1 kcal/mol. Ertl et al. is ref 10, King et al. is ref 11, and Campbell et al. is ref 12. GGA-RPA is ref 5 and M06-L is ref 9. The value of King et al. is also shown according to the suggested correction of Campbell et al. The calculated binding energy from DFT at the GGA-RPA level underestimates the experimental values by 5 kcal/mol. A DFT calculation based on the meta-generalized M06-L functional is in better agreement with the experimental values. The theoretical values were corrected to the difference in zero point energies of the gas-phase molecule and the adsorbate.

other methods. The isosteric heat of adsorption of Ertl et al.,[10] derived from adsorption isotherms, as well as the value of Campbell and co-workers,[12] obtained by microcalorimetry, agree reasonably well with our results. A second microcalorimetry measurement from King et al. does not agree with our result. Indeed it appears to be an outlier when compared to all other experiments. The authors of refs 12 and 28 showed that an error in the calibration of the calorimeter is responsible for deviations in the King work and estimated a correction (~40%), also shown in Figure 10, which brings it into better agreement with our results.

Table 2 compares the derived binding energies of this work to predictions of several DFT calculations. All calculations are within 0.6 eV of the experimental value reported in this work. Calculations based on LDA functionals overbind CO to Pt(111) by more than 0.5 eV, whereas use of the BLYP functional (with a strong gradient correction) underbinds by a similar amount. The reason for this strong variation of the binding energy for different XC functionals is that GGA functionals artificially stabilize the surface and therefore weaken


DOI: 10.1021/ja509530k
J. Am. Chem. Soc. 2015, 137, 1465−1475

Table 2. Comparison of the Binding Energies for CO/Pt(111) Derived From TST to the Theoretical Predictions From DFT Calculations[a]

| binding energy | | | |
|---|---|---|---|
| eV | kcal/mol | method | reference |
| 1.47 ± 0.04[b] | 34 ± 1 | velocity-resolved residence time | this work |
| 1.40 | 32.2 | adsorption isotherms | 10 |
| 1.94 | 44.7 | microcalorimetry | 11 |
| 1.35 | 31.1 | microcalorimetry | 12 |
| | | Theoretical | |
| 1.40 | 32.3 | M06-L | 9 |
| 1.23 | 28.4 | PBE-RPA | 5 |
| 1.27−1.32 | 29.3−30.4 | RPBE | 3b |
| 1.37 | 31.6 | DFT-GGA | 6c |
| 1.32−1.44 | 30.4−33.2 | PW91 | 6a |
| 0.93 | 21.4 | BLYP | 5 |
| 1.23 | 28.4 | RPBE | 5 |
| 1.78 | 41.0 | HSE | 5 |
| 1.85 | 42.7 | AM05 | 5 |
| 1.99 | 45.9 | PBEsol | 5 |
| 1.50 | 34.6 | revTPSS | 6b |

[a]Note that we derive $D_0$ (energy difference between the lowest states) values, whereas the theoretical calculation generally gives values for $D_e$ (energy difference between the bottoms of the potentials). Therefore, we subtracted the difference in zero point energy (~0.08 eV) from the reported theoretical values to make them comparable to the experimental results. [b]Average of $D_0^{osc}$ and $D_0^{2D}$; see text.

the CO−metal bond.[5] In general, it has been observed that LDA-DFT yields reasonably good lattice constants but fails to describe binding energies. In contrast, GGA-DFT gives better values for the binding energy but overestimates lattice constants.[6b] One of the best possible DFT calculations available uses GGA XC functionals in combination with the random phase approximation (RPA). Schimka et al. showed that PBE-RPA calculations succeed to predict the correct binding site for CO on Pt(111).[5] There is still a substantial difference between the binding energy from that work and our recommendation. One should note that the experimental results of Figure 10 are for the zero coverage limit. The PBE-RPA calculations of ref 5 were carried out with a 2 × 2 super-cell and due to the use of periodic boundary conditions may reflect better the binding energy of CO to Pt(111) when coverage is 0.25 ML, which is expected to be less than that at zero coverage. We have made no effort to account for this in the present comparison. Calculations of Luo et al. showed that the correct site preference as well as reasonable lattice constants, surface energies, and binding energies can be obtained with the meta-generalized M06-L XC functional.[9] Results using M06-L are in significantly better agreement with experiment than PBE-RPA.

## CONCLUSIONS AND OUTLOOK

In conclusion, we investigated the desorption kinetics of CO molecules from a Pt(111) crystal with 0.5−1% step density. We employed a new velocity-selected residence time measurement, which uses a double-resonance detection scheme to suppress the influence of desorbed CO's velocity distribution on the time-dependent data. This enables us to perform experiments that are exclusively sensitive to residence time, with high signal-to-noise ratio and temporal resolution. We used intense pulsed molecular beams that allow initial doses as high as 3% ML, significantly higher than the step density. We demonstrate that under these conditions, the desorption kinetics of CO from the Pt(111) surface is bi-exponential in the temperature range, $T_S$ = 582−713 K. This is due to the fact that the kinetics of CO desorption from Pt(111) are intrinsically influenced by steps. With the help of a previously introduced kinetic model involving terrace adsorption and desorption as well as diffusion between terraces and steps, we are able to assign the two processes to direct terrace desorption (fast) and step-to-terrace diffusion followed by desorption (slow). We compared our results to four previous molecular beam studies, which all reported single exponential kinetics but disagree on the magnitude of the rate constants. It appears that the deviation between these various experiments can be attributed to the influence of steps on the desorption kinetics, which is difficult to control and detect in experiments.

We applied TST to derive a binding energy for CO adsorption at Pt(111) terraces. Our results are in good agreement with previous heat of adsorption measurements based on calorimetry and isosteric heats. High-level DFT calculations employing GGA and RPA underestimate our results by ~5 kcal/mol, whereas calculations using the meta-generalized M06-L function are in better agreement with the experimental values.

Finally, we emphasize that the velocity-selected residence time measurements can be extended to other molecule−surface systems. In its current design, our experiment is limited to molecules that have a metastable intermediate state that can be used for tagging and velocity filtering. However, the implementation of velocity map imaging (VMI) together with other laser-based ionization methods, e.g., one photon VUV ionization or multiphoton ionization with fs lasers, can make this approach more generally applicable. Furthermore, it would be useful to improve the temporal resolution of the experiment by using shorter molecular beam pulses to extend the range of surface temperatures; in this work the pulse duration was an unspectacular 150 μs, but intense pulsed beam sources with 10 μs duration are commercially available.

## ASSOCIATED CONTENT

### Supporting Information

Supporting material contains the analytical solutions of the differential rate eqs 2−5 for $N_{ad}(t)$, $N_{ad}^{(1)}(t)$, and $N_{ad}^{(2)}(t)$ . This material is available free of charge via the Internet at http://pubs.acs.org.

## AUTHOR INFORMATION

### Corresponding Author

christof.bartels@mpibpc.mpg.de

### Notes

The authors declare no competing financial interest.

## ACKNOWLEDGMENTS

We thank Sebastian Schnell and Dr. Martin Wenderoth for their kind assistance with atomic force microscopy, as well as Hartmut Sebesse for creating the graphical abstract. We wish to acknowledge Dr. Philippe Sautet for useful discussions on the RPA method. A.M.W. and C.B. acknowledge support from the Alexander von Humboldt foundation.

## REFERENCES

(1) Ertl, G. *Angew. Chem., Int. Ed. Engl.* **1990**, *29* (11), 1219−1227.
(2) Tully, J. C. *Surf. Sci.* **1994**, *299* (1−3), 667−677.



DOI: 10.1021/ja509530k
J. Am. Chem. Soc. 2015, 137, 1465−1475

(3) (a) Hammer, B.; Nørskov, J. K. In *Advances in Catalysis*; Bruce, C. Gates, H. K., Ed. Academic Press: San Diego, CA, 2000; Vol. *45*, pp 71−129. (b) Peterson, A. A.; Grabow, L. C.; Brennan, T. P.; Shong, B. G.; Ooi, C. C.; Wu, D. M.; Li, C. W.; Kushwaha, A.; Medford, A. J.; Mbuga, F.; Li, L.; Norskov, J. K. *Top. Catal.* **2012**, *55* (19−20), 1276−1282. (c) Hammer, B.; Morikawa, Y.; Nørskov, J. K. *Phys. Rev. Lett.* **1996**, *76* (12), 2141−2144.
(4) Feibelman, P. J.; Hammer, B.; Nørskov, J. K.; Wagner, F.; Scheffler, M.; Stumpf, R.; Watwe, R.; Dumesic, J. *J. Phys. Chem. B* **2000**, *105* (18), 4018−4025.
(5) Schimka, L.; Harl, J.; Stroppa, A.; Gruneis, A.; Marsman, M.; Mittendorfer, F.; Kresse, G. *Nat. Mater.* **2010**, *9* (9), 741−744.
(6) (a) Gil, A.; Clotet, A.; Ricart, J. M.; Kresse, G.; Garcia-Hernandez, M.; Rosch, N.; Sautet, P. *Surf. Sci.* **2003**, *530* (1−2), 71−86. (b) Sun, J. W.; Marsman, M.; Ruzsinszky, A.; Kresse, G.; Perdew, J. P. *Phys. Rev. B* **2011**, *83* (12), 121410. (c) Hammer, B.; Morikawa, Y.; Norskov, J. K. *Phys. Rev. Lett.* **1996**, *76* (12), 2141−2144. (d) Hu, Q. M.; Reuter, K.; Scheffler, M. *Phys. Rev. Lett.* **2007**, *98* (17), 176103. (e) Ren, X. G.; Rinke, P.; Scheffler, M. *Phys. Rev. B* **2009**, *80* (4), 045402.
(7) (a) Blackman, G. S.; Xu, M. L.; Ogletree, D. F.; Vanhove, M. A.; Somorjai, G. A. *Phys. Rev. Lett.* **1988**, *61* (20), 2352−2355. (b) Ogletree, D. F.; Vanhove, M. A.; Somorjai, G. A. *Surf. Sci.* **1986**, *173* (2−3), 351−365. (c) Steininger, H.; Lehwald, S.; Ibach, H. *Surf. Sci.* **1982**, *123* (2−3), 264−282. (d) Hayden, B. E.; Kretzschmar, K.; Bradshaw, A. M.; Greenler, R. G. *Surf. Sci.* **1985**, *149* (2−3), 394−406.
(8) Zhao, Y.; Truhlar, D. G. *J. Chem. Phys.* **2006**, *125* (19), 194101.
(9) Luo, S. J.; Zhao, Y.; Truhlar, D. G. *J. Phys. Chem. Lett.* **2012**, *3* (20), 2975−2979.
(10) Ertl, G.; Neumann, M.; Streit, K. M. *Surf. Sci.* **1977**, *64* (2), 393−410.
(11) Yeo, Y. Y.; Vattuone, L.; King, D. A. *J. Chem. Phys.* **1997**, *106* (1), 392−401.
(12) Fischer-Wolfarth, J. H.; Hartmann, J.; Farmer, J. A.; Flores-Camacho, J. M.; Campbell, C. T.; Schauermann, S.; Freund, H. J. *Rev. Sci. Instrum.* **2011**, *82* (2), 024102.
(13) (a) Verheij, L. K.; Lux, J.; Anton, A. B.; Poelsema, B.; Comsa, G. *Surf. Sci.* **1987**, *182* (3), 390−410. (b) Lin, T. H.; Somorjai, G. A. *Surf. Sci.* **1981**, *107* (2−3), 573−585. (c) Campbell, C. T.; Ertl, G.; Kuipers, H.; Segner, J. *Surf. Sci.* **1981**, *107* (1), 207−219. (d) Winicur, D. H.; Hurst, J.; Becker, C. A.; Wharton, L. *Surf. Sci.* **1981**, *109* (1), 263−275.
(14) Serri, J. A.; Cardillo, M. J.; Becker, G. E. *J. Chem. Phys.* **1982**, *77* (4), 2175−2189.
(15) (a) Serri, J. A.; Tully, J. C.; Cardillo, M. J. *J. Chem. Phys.* **1983**, *79* (3), 1530−1540. (b) Reutt-Robey, J. E.; Doren, D. J.; Chabal, Y. J.; Christman, S. B. *Phys. Rev. Lett.* **1988**, *61* (24), 2778−2781.
(16) Starr, D. E.; Campbell, C. T. *J. Am. Chem. Soc.* **2008**, *130* (23), 7321−7327.
(17) Ran, Q.; Matsiev, D.; Wodtke, A. M.; Auerbach, D. J. *Rev. Sci. Instrum.* **2007**, *78* (10), 104104.
(18) Gilijamse, J. J.; Hoekstra, S.; Meek, S. A.; Metsälä, M.; van de Meerakker, S. Y. T.; Meijer, G.; Groenenboom, G. C. *J. Chem. Phys.* **2007**, *127* (22), 221102.
(19) Hermann, K., In *Crystallography and Surface Structure*; Wiley-VCH Verlag GmbH & Co. KGaA: Weinheim, Germany, 2011; pp 265−266.
(20) Yoon, M.; Mochrie, S. G. J.; Zehner, D. M.; Watson, G. M.; Gibbs, D. *Surf. Sci.* **1995**, *338* (1−3), 225−235.
(21) (a) Campbell, C. T.; Ertl, G.; Kuipers, H.; Segner, J. *J. Chem. Phys.* **1980**, *73* (11), 5862−5873. (b) Harris, J.; Luntz, A. C. *J. Chem. Phys.* **1989**, *91* (10), 6421−6428. (c) Hayden, B. E.; Bradshaw, A. M. *Surf. Sci.* **1983**, *125* (3), 787−802. (d) Hayden, B. E.; Bradshaw, A. M. *J. Electron Spectrosc.* **1983**, *30* (Feb), 51−51. (e) Hopster, H.; Ibach, H. *Surf. Sci.* **1978**, *77* (1), 109−117. (f) Norton, P. R.; Goodale, J. W.; Selkirk, E. B. *Surf. Sci.* **1979**, *83* (1), 189−227.
(22) Lin, T. H.; Somorjai, G. A. *Surf. Sci.* **1981**, *107* (2−3), 573−585.
(23) Poelsema, B.; Verheij, L. K.; Comsa, G. *Phys. Rev. Lett.* **1982**, *49* (23), 1731−1735.
(24) Stuckless, J. T.; Starr, D. E.; Bald, D. J.; Campbell, C. T. *Phys. Rev. B* **1997**, *56* (20), 13496−13502.
(25) Gdowski, G. E.; Madix, R. J. *Surf. Sci.* **1982**, *115* (3), 524−540.
(26) Lahee, A. M.; Toennies, J. P.; Woll, C. *Surf. Sci.* **1986**, *177* (2), 371−388.
(27) (a) Hanggi, P.; Talkner, P.; Borkovec, M. *Rev. Mod. Phys.* **1990**, *62* (2), 251−341. (b) Truhlar, D. G.; Garrett, B. C.; Klippenstein, S. J. *J. Phys. Chem.* **1996**, *100* (31), 12771−12800. (c) Ju, L.-P.; Han, K.-L.; Zhang, J. Z. H. *J. Comput. Chem.* **2009**, *30* (2), 305−316.
(28) Karp, E. M.; Campbell, C. T.; Studt, F.; Abild-Pedersen, F.; Nerskov, J. K. *J. Phys. Chem. C* **2012**, *116* (49), 25772−25776.
(29) Poelsema, B.; Palmer, R. L.; Comsa, G. *Surf. Sci.* **1984**, *136* (1), 1−14.
(30) Collins, D. M.; Spicer, W. E. *Surf. Sci.* **1977**, *69* (1), 85−113.
(31) McCabe, R. W.; Schmidt, L. D. *Surf. Sci.* **1977**, *65* (1), 189−209.


DOI: 10.1021/ja509530k
*J. Am. Chem. Soc.* 2015, 137, 1465−1475